

# Synthesis of micrometer-size poly(*N*-isopropylacrylamide) microgel particles with homogeneous crosslinker density and diameter control

Tim Still<sup>a,b,\*</sup>, Ke Chen<sup>c</sup>, Ahmed M. Alsayed<sup>b</sup>, Kevin B. Aptowicz<sup>d</sup>, A.G. Yodh<sup>a</sup>

<sup>a</sup> Department of Physics and Astronomy, University of Pennsylvania, Philadelphia, PA 19104, USA

<sup>b</sup> Complex Assemblies of Soft Matter, CNRS-Rhodia-UPenn, UMI 3254, USA

<sup>c</sup> Beijing National Laboratory for Condensed Matter Physics and Key Laboratory of Soft Matter Physics, Institute of Physics, Chinese Academy of Sciences, Beijing 100190, China

<sup>d</sup> Department of Physics, West Chester University, West Chester, PA 19383, USA

## ARTICLE INFO

### Article history:

Received 19 December 2012

Accepted 17 May 2013

Available online 31 May 2013

### Keywords:

Colloids

Polymers

Hydrogels

Synthesis

Thermoresponsive

## ABSTRACT

Poly(*N*-isopropylacrylamide) microgel particles are synthesized using a semi-batch surfactant-free emulsion polymerization method. Particle diameter can be precisely adjusted by controlling the initial conditions, the electrolyte concentration, and the monomer feeding rate and duration. Larger particles are obtained in the presence of small amounts of co-monomer with cationic amino groups that compete against the negative charges arising from the initiator. Monodisperse particles with uniform cross-linker density, homogeneous optical properties, and pronounced thermoresponsivity are readily produced with a wide variety of diameters ranging from several hundred nanometers to a few micrometers. The charge stabilization mechanisms that control particle growth are discussed.

© 2013 Elsevier Inc. All rights reserved.

## 1. Introduction

Hydrogel particles composed of crosslinked poly(*N*-isopropylacrylamide) (PNIPAM) have been intensely studied over the last decade, in large measure because they undergo a reversible volume transition as a function of temperature. PNIPAM polymer has a lower critical solution temperature of  $\approx 32^\circ\text{C}$  in water, and colloidal spheres made of PNIPAM chains and crosslinked with *N,N'*-methylenebisacrylamide (BIS) shrink in diameter with increasing temperature. This simple effect has led to a variety of applications for these particles, for example, as drug delivery agents [1], mechanical oscillators [2], biosensors [3,4], and as the key constituents of model colloids for the study of fundamental statistical physics [5–11]. Besides application, full elucidation of the novel chemical, structural, and rheological properties of PNIPAM microgel particles remains fundamentally interesting and continues to be investigated [12–22].

Many of the aforementioned applications and experiments require optical microscopy and particle tracking of PNIPAM particles. Optimally, PNIPAM particle size must be in the  $\mu\text{m}$ -range in order to be both visible by optical microscopy and influenced by thermal fluctuations. In such optical experiments, a uniform refractive index across the particle is often desired. Similarly, control and knowl-

edge of the polymer cross-linker distribution within the particles is desirable, because many applications and experiments depend on homogeneous microgel particle mechanical properties. Unfortunately, conventional PNIPAM synthesis delivers particles with heterogeneous optical and mechanical properties as a result of different monomer and crosslinker kinetics during polymerization.

To this end, we introduce and demonstrate a combination of synthetic strategies, including semi-batch synthesis, co-polymerization, and salt concentration manipulation, to produce uniformly crosslinked and optically homogeneous PNIPAM particles with precise control of particle size in the  $\approx 800\text{ nm}$  to  $4\ \mu\text{m}$  range. We anticipate that the resulting enhanced command over these properties will make preparation of colloidal suspensions easier and will therefore lead to improved application and experimentation with these novel colloidal materials.

Typically, PNIPAM particles are synthesized by surfactant-free radical emulsion polymerization of *N*-isopropylacrylamide (NIPAM) and BIS in water at  $60\text{--}80^\circ\text{C}$  using water-soluble initiators such as ammonium peroxydisulfate (APS). APS forms a water-soluble radical that initiates a NIPAM monomer, which then starts a polymer chain. When the PNIPAM chain grows beyond a critical length, phase separation occurs because of the polymer's insolubility in water at the reaction temperature. The resulting colloidal particles are stabilized by the charge from initiator molecules, e.g., the sulfate groups of APS. Note, the use of additional surfactant, e.g., sodium dodecyl sulfate, can sometimes improve stability [23].

\* Corresponding author at: Department of Physics and Astronomy, University of Pennsylvania, Philadelphia, PA 19104, USA.

E-mail address: timstill@seas.upenn.edu (T. Still).

In practice, the crosslinker reacts faster than NIPAM at the typical reaction temperatures, and, as a result, an inhomogeneous crosslinking density in the microgel particles is produced [23]. When the crosslinking density is higher at the center of the particles, the polymer density in the swollen state is also higher, which, in turn, can adversely influence particle mechanical and optical properties [24]. One approach has been devised to reduce these inhomogeneities; it employs a semi-batch procedure. With this approach, homogeneous, nearly transparent *small* microgel particles with diameters of a few hundred nm have been obtained [24,25].

Of course, it is well known that particle size is influenced by other parameters, including initial monomer concentration, temperature, monomer-to-crosslinker ratio, and initiator concentration. For typical reaction conditions, particle size is restricted to diameters below 1  $\mu\text{m}$ , and the addition of surfactants such as sodium dodecyl sulfate leads to a further decrease of particle diameter compared to surfactant-free polymerization methodologies [23]. Other schemes have been explored to increase particle size while maintaining functionality. For example, particles larger than 1  $\mu\text{m}$  can be prepared by adding electrolytes to the solution during the polymerization in one-pot syntheses [26], and particle size can be controlled by the electrolyte concentration, albeit at the cost of increased polydispersity. Yet another approach adds small amounts of co-monomers into the suspensions. Acrylic acid co-monomer leads to highly charged particles, but these particles no longer exhibit a strong temperature-dependence [27,29]. 2-Aminoethylmethacrylate hydrochloride (AEMA) has also been used as a co-monomer, adding positively charged amine groups to the particle surface [30,5,29]. Such particles range between 1 and 2  $\mu\text{m}$  in diameter, are highly temperature-responsive, and the additional amine groups can be used to further functionalize the particles, e.g., with dye molecules; particle size, however, is not optimally controlled in these processes even under well-managed experiment conditions.

Herein, we present a simple synthesis scheme to make near-transparent, homogeneously crosslinked, micrometer-sized spheres. A semi-batch method, with or without AEMA as co-monomer and with or without the addition of electrolytes, is demonstrated to yield uniform PNIPAM spheres with well controlled diameter ranging between 0.8 and 4  $\mu\text{m}$ . The reaction can be easily altered to meet individual demands, and the growth rate is easily controlled. We show that the particles grow linearly with reaction time, permitting experimenters to predictably stop the reaction when a desired particle diameter has been reached.

## 2. Experimental section

(a) *with AEMA*. NIPAM (Polysciences) was recrystallized in hexane. BIS, AEMA (both Polysciences) and APS (Sigma–Aldrich, 98%) were used without further purification. 2.00 g NIPAM (17.7 mmol), 50 mg BIS (0.32 mmol), and 8.6 mg AEMA (0.05 mmol) were dissolved in 50 mL filtered, deionized water ( $R > 18 \text{ M}\Omega$ ) in a three-neck flask equipped with a mechanical stirrer and purged with nitrogen for 20 min. Thirty milliliter of this solution was then filled in a syringe. Ten milliliter water was added to the remaining 20 mL solution in the flask, and the liquid was heated to 80  $^{\circ}\text{C}$  and purged with nitrogen. The polymerization was initiated by addition of 10.4 mg APS (0.05 mmol) dissolved in 2 mL water. After about 4 min, when the solution started to become turbid, the solution in the syringe was fed in the reaction vessel at a rate of 1 mL/min (using a Harvard Apparatus 11plus syringe pump); 0.1 mL of the reaction mixture was taken out every 3–6 min and quenched in ice water. 5 min after all solution was added, the reaction was stopped and the colloidal suspension was cooled down rapidly

below room temperature in an ice bath. A schematic drawing of the setup is shown in Fig. 1c.

The reaction was repeated twice with identical concentrations and under identical conditions unless that initially 120 mL (or 35 mL, respectively) solution were prepared out of which 100 mL (15 mL) were fed in the reaction over 100 min (15 min) at 1 mL/min.

(b) *lower initial concentration of educts*. 50 mL of an identical solution like in experiment (a) was prepared. This time, a syringe was filled with 40 mL of the solution, and the 10 mL remaining in the flask were diluted with 20 mL of water, so that the initial concentrations of monomer, AEMA, and crosslinker were reduced by a factor of two. Under the same conditions as in (a), the reaction was started by addition of 10 mg APS in 2 mL water and the feeding was done at 1 mL/min for 40 min.

(c) *without AEMA*. The experiment was repeated with identical concentrations and under identical conditions as in (a) absent the AEMA. Another synthesis was performed at lower initial concentration like in (b).

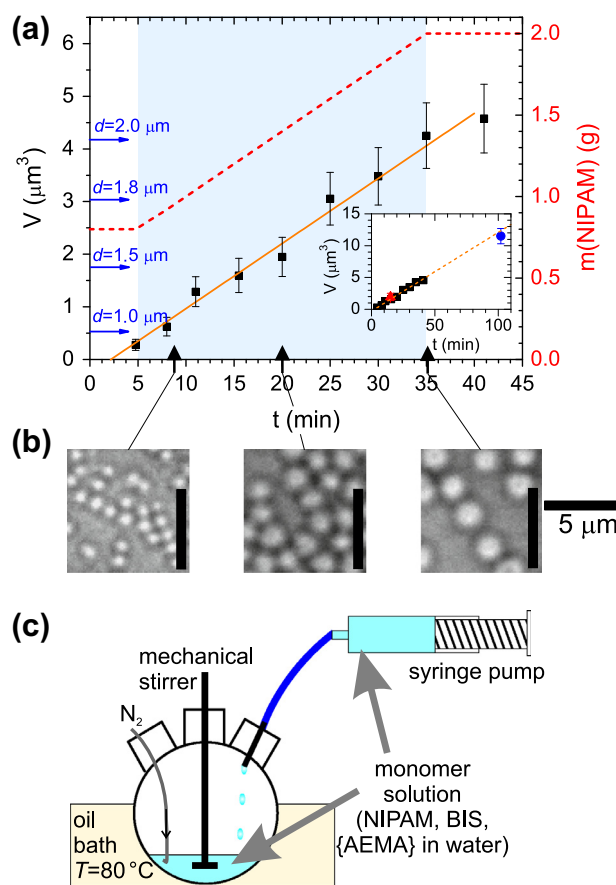


**Fig. 1.** (a) Volume of PNIPAM spheres as a function of reaction time. Feeding of the monomer solution in the semi-batch process starts after 5 min and continues for 30 min (light blue shaded region), and the volume of the individual particles varies linearly with time (solid orange line). The corresponding particle diameter ( $d \propto V^{1/3}$ ) is indicated by horizontal arrows. The dashed red line (right side scale) shows the total amount of NIPAM monomer (i.e., reacted plus unreacted monomer) in the reaction vessel. The inset compares the reaction (black squares) to two additional batches under otherwise identical reaction conditions but with different total feeding volumes of 15 mL (red triangle) and 100 mL (red circle), respectively. The linear particle growth is reproduced in these syntheses. All error bars correspond to an uncertainty of  $\pm 100$  nm in the particle diameter. (b) Exemplary micrographs of particles quenched at different reaction times, indicated by small vertical arrows in (a). (c) Schematic drawing of the semi-batch synthesis setup. (For interpretation of the references to colour in this figure legend, the reader is referred to the web version of this article.)

(d) with sodium chloride. The experiment was repeated with identical concentrations and under identical conditions as in (c) but the electrolyte concentration was increased by adding 20 mg NaCl (0.34 mmol, 1 wt.% relative to NIPAM).

### 2.1. Microscopy

Standard brightfield microscopy was performed with a Zeiss Axiovert 135 utilizing a 100 $\times$  oil objective, a Uniq camera, and an objective heater (BiOptechs, accuracy  $\pm 0.1$  °C) [5,28,9]. PNIPAM samples were prepared by confining small drops (ca. 0.6  $\mu$ L) of the colloidal suspension between two cover slips.

### 2.2. Light scattering

Static light scattering experiments were performed on a Brookhaven Instruments setup, utilizing a green ( $\lambda = 514.5$  nm, 35 mW) laser. Temperature was controlled by a thermostat with an accuracy of  $\pm 0.1$  °C. Static light scattering was measured at angles between 15° and 60° at low hydrogel concentrations (<0.01 wt.%). Dynamic light scattering was measured utilizing a ProteinSolutions DynaPro setup ( $\lambda \approx 800$  nm, 60 mW) at temperatures between 19 °C and 45 °C.

### 2.3. Zeta potential

The  $\zeta$ -potential was measured at 25 °C using a Beckman Coulter Delsa Nano C, diluted in filtered DI water ( $R > 18$  M $\Omega$ ).

## 3. Results and discussion

### 3.1. Particle growth

For each synthesis, the geometric diameters of the particles that were quenched at different times were measured by microscopy at  $T = 22$  °C, averaging over at least 40 particles. Typical micrographs can be seen in Fig. 1b for PNIPAM spheres with AEMA (as described in paragraph (a) of the synthesis section). The corresponding particle volume,  $V$ , as a function of reaction time,  $t$ , is shown in Fig. 1a; horizontal arrows indicate the particle diameter corresponding to particular PNIPAM particle volumes. Notice, the particle volume grows linearly with the reaction time during the entire feeding period (light blue background), i.e., between  $t = 5$ –35 min. The same behavior was found for the two identical syntheses but with different feeding volume, as plotted in the inset of Fig. 1a. It is clear that the final particle size is determined by the total feeding volume when all other conditions are the same.

The particle growth also mirrors the total amount of NIPAM monomer fed into the reaction. This effect is shown by the dashed red line in Fig. 1a (right scale). This phenomenon is due to the fast kinetics of the NIPAM polymerization at high temperatures after the initial period when the colloidal seeds collapse [23]. In essence, most of the monomer (NIPAM and crosslinker BIS) polymerizes nearly instantaneously (with the growing seeds) after it is added to the reaction vessel, and thus the growth rate depends largely on the feeding rate. The net result is linear particle growth that mirrors the temporally linear addition of monomer.

Starved-feed conditions in the semi-batch synthesis of PNIPAM at 80 °C were confirmed by monitoring the monomer conversion in Ref. [25], in agreement with trends seen in previous kinetic experiments [23]. In fact, the linear growth in all syntheses shown in Fig. 2 provides strong evidence that our experiment indeed fulfills these conditions. Moreover, the fact that the growth is linear with respect to particle size in the swollen state, implies an essentially constant swelling ratio for particles quenched at all stages during

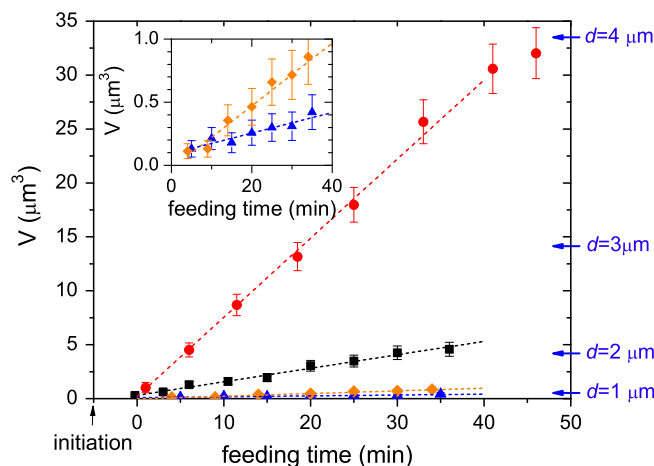


**Fig. 2.** Semi-batch PNIPAM polymerization under different conditions: with AEMA (black squares), with AEMA and lowered initial concentration (red circles), without AEMA (blue triangles), and without AEMA with NaCl (orange diamonds). For comparison, the two samples without AEMA are shown in the inset on a smaller volume scale. All particles grow linearly in volume over the entire feeding time. Particle size is measured at 22 °C. (For interpretation of the references to colour in this figure legend, the reader is referred to the web version of this article.)

the reaction. The swelling ratios,  $d_{20^\circ\text{C}}/d_{45^\circ\text{C}}$ , of the final particles (see Table 1) were measured by dynamic light scattering and were found to be virtually independent of the presence/absence of AEMA for particles of similar diameter.

The same argument holds for particles synthesized under all of the conditions described in the synthesis section. Note, however, the growth slope varies dramatically between the syntheses schemes (a–d) as shown in Fig. 2. Here, in order to account for slightly different initiation times, i.e., between 3 and 6 min until the suspension became cloudy, Fig. 2 shows  $V(t)$  as a function of feeding time, i.e.,  $t = 0$  is when feeding starts. Reducing the initial concentration of educts (red circles, synthesis (b)), while keeping the amount of initiator constant leads to a much faster growth of the individual particles. On the other hand, without AEMA (blue triangles, synthesis (c), and orange diamonds, with NaCl, synthesis (d)), the growth rates are much slower. Since the polymerization kinetics should not be significantly influenced by the varied conditions, these findings must result from different numbers of growing colloidal particles for each condition.

The key to understanding the observed differences is the charge stabilization of the growing spheres. Initially, NIPAM and BIS monomer are dissolved in water at 80 °C. The polymerization is started by the addition of the water-soluble initiator APS, leading to growing PNIPAM chains in solution. These growing chains become more and more hydrophobic and, at a critical chain length, the chains precipitate and agglomerate to form primary seeds [26]. These seeds further agglomerate until they become colloidal stable; stabilization results from charge on the colloidal surface. The charges originate from the sulfonate groups of the initiator (negative) or from the amine groups of AEMA (positive). The primary seeds agglomerate until the resulting particles have accumulated enough charges to prevent further coagulation [31]. Once the number of stable seeds is established, it remains constant, and the particles grow homogeneously (equilibrium phase). It is noteworthy that the synthesis at 80 °C has been empirically found to deliver more uniform and less “sticky” (in terms of microscopy experiments on glass substrates) particles compared to particles synthesized at lower temperatures [29].

The conditions in the syntheses (a–d) require different amounts of charge for each particle seed to become stable. In particular, in the absence of AEMA, the only charges to stabilize the seed are the sulfonate groups of the initiator. Addition of an electrolyte like

**Table 1**Summary of initial conditions, final diameter, swelling ratio  $d_{20^\circ\text{C}}/d_{45^\circ\text{C}}$ , and zeta potential for PNIPAM particles prepared by syntheses (a–d).

	$V(\text{H}_2\text{O})$	$m(\text{NIPAM})$	$m(\text{BIS})$	$m(\text{AEMA})$	$m(\text{APS})$	$m(\text{NaCl})$	$d_{20^\circ\text{C}}$	$d_{20^\circ\text{C}}/d_{45^\circ\text{C}}$	$\zeta$ -potential
(a)	50 + 10 mL	2.00 g	50 mg	8.6 mg	10.4 mg	–	$2.1 \pm 0.2 \mu\text{m}$	$\approx 2.0$	+2.2 mV
(b)	50 + 20 mL	2.00 g	50 mg	8.6 mg	10.4 mg	–	$3.8 \pm 0.2 \mu\text{m}$	$\approx 2.7$	+4.6 mV
(c)	50 + 10 mL	2.00 g	50 mg	–	10.4 mg	–	$1.0 \pm 0.2 \mu\text{m}$	$\approx 2.1$	–10.3 mV
(d)	50 + 10 mL	2.00 g	50 mg	–	10.4 mg	20 mg	$1.3 \pm 0.2 \mu\text{m}$	$\approx 2.2$	–8.4 mV

NaCl leads to a screening of these charges, resulting in a lower repulsion between aggregating seeds, which causes more primary seeds to agglomerate before colloidal stability is reached. Correspondingly, the number of stable growing particles is lower in the presence of electrolyte and the additional monomer reacts with less particles, leading to a faster growth per particle and, thus, larger particles [26]. The significance of this effect is highlighted in the inset of Fig. 2, showing that the slope of the  $V(t)$  curve approximately doubles by addition of 1 wt.% NaCl relative to NIPAM; this corresponds to a diameter that is approximately 25% larger.

Larger particles are obtained in the presence of AEMA. In this case, the particles are stabilized by the positively charged amine group [30], but the stabilization effect is reduced by the simultaneous presence of the negative sulfate groups. Therefore, the primary seeds agglomerate into a few larger particles until the excess of amine groups over sulfate groups is sufficiently large, and a positive net charge stabilizes the seeds. Accordingly, we find negative zeta potentials in syntheses without AEMA and positive zeta potentials in the presence of AEMA co-monomer (cf. Table 1). It is noteworthy that because of this balance between positive and negative charges, some ratios of AEMA monomer to APS initiator do not produce stable colloids. Taking only half of the AEMA used in syntheses (a) and (b), for example, leads to the agglomeration of all the PNIPAM during the polymerization and colloidal particles are not produced. In this context, it is noteworthy that using the same molar amount of AEMA and APS in syntheses (a) and (b) still leads to a positive surface charge, although the initiator can, in principle, deliver two negative charges per mole, whereas AEMA only delivers one positive charge per mole. The reason behind this observation is that even at  $80^\circ\text{C}$ , the thermal decomposition of persulfate initiator is relatively slow ( $t_{1/2} \approx 2 \text{ h}$  [Sigma–Aldrich product information]), i.e., the contribution of AEMA to the colloid's surface charge is dominant under the present experimental conditions.

The addition of AEMA to an otherwise identical synthesis (synthesis (a) vs. (c)) leads to particles that are about an order of magnitude larger in volume (i.e., more than a factor two larger in diameter). Interestingly, reducing the initial concentration of the monomers in synthesis (b) further increases the volume of the resulting particles by a factor of  $\approx 7$ , whereas the same reduction leads to essentially the same particle diameter in the absence of AEMA (not shown). Therefore, it is unlikely that the number density of growing chains directly after initiation plays an important role in the process, and, again, charge stabilization must be assumed as the reason for the large particles created in synthesis (b). It should be noted that unlike all monomers including AEMA, the concentration of the initiator APS was held constant between (a) and (b). Hence, the number of initial radicals and primary seeds is similar in both cases, but in the presence of AEMA, a sufficient amount of positive charge to balance the sulfate groups and stabilize the seeds are only obtained when enough AEMA molecules are copolymerized into the growing chains of the agglomerating seeds. Correspondingly, the equilibrium phase is reached at later reaction times, and the number of growing particles is much lower, resulting in larger particles.

A rough estimation of the number of stable seeds can be obtained from the final particle size in the collapsed state from

$N = 2.0 \text{ g}/(4/3\pi r_{45^\circ\text{C}}^3(1 - c_{\text{H}_2\text{O}})1.27 \times 10^6 \text{ g/m}^3)$ , where  $r_{45^\circ\text{C}}$  is the radius in the collapsed state and  $c_{\text{H}_2\text{O}}$  is the relative content of entrapped water in the collapsed microgels.  $c_{\text{H}_2\text{O}}$  was measured to between  $\approx 75\%$  [32] and  $\approx 40\%$  [33], but lower estimates of 25% have been reported [13]. If we assume  $c_{\text{H}_2\text{O}} \approx 50\%$ , then we find  $N$  to vary between  $2.2 \times 10^{12}$  (synthesis (b)) and  $4.9 \times 10^{13}$  (synthesis (c)); synthesis (a) was  $5.7 \times 10^{12}$  and synthesis (d) was  $2.8 \times 10^{13}$ . We note that  $c_{\text{H}_2\text{O}}$  could vary with surface charge [32], so further experimentation would be needed to obtain a more reliable estimation of  $N$  for each particle species.

Since the particle growth can be controlled by the feeding rate (which we kept constant in this study), the particles grow slowly and very uniformly. As a result, the particles are very monodisperse, with some small amount of secondary nucleation only for the largest particles (syntheses (a) and (b)), which can easily be removed by centrifugation. A uniform particle size is achieved even in the presence of electrolytes, which is an important advantage over the corresponding one-pot synthesis, which usually yields polydisperse samples [26]. The uniformity of the particles prepared by synthesis (d) is clearly depicted by their tendency to form quasi-two-dimensional colloidal crystals as shown in Fig. 3a. The analysis of such quasi-two-dimensional micrographs using standard particle tracking techniques [34] permits an estimation of the polydispersity,  $p = 0.02\text{--}0.05$ , in agreement with dynamic light scattering; static light scattering, on the other hand, measures somewhat higher polydispersities ( $p \approx 0.1$ , see following section).

It should be noted that the employment of surfactant in the semi-batch synthesis described in Ref. [25] leads to a much slower particle growth because the surfactant stabilizes more and smaller seeds in the initial phase of the reaction. At long reaction times (compared to our synthesis), which correspond to similar diameters as the smallest  $d$  measured in our experiment, the authors find the same linear  $V(t)$  dependence as presented in Fig. 1 and excellent monodispersity.

### 3.2. Optical properties

It is well-known that the crosslinker BIS polymerizes faster than NIPAM, leading to a heterogeneous crosslinking-density in PNIPAM colloidal particles synthesized following the classical one-pot route [23]. Based on the observations of previous scattering experiments [14,24,35–39], a picture emerges of a particle whose polymer chains are highly crosslinked in its core, while at the surface, the structure is “hairy” [40,30,41]. In accordance with that picture, the microgel is often described as a homogeneously crosslinked core with a weakly crosslinked soft outer shell [14,37,24,42,25]. Free chains at the interface account for additional steric stabilization of PNIPAM colloids at low temperatures.

Importantly, our continuous addition of monomer and crosslinker results in a uniform crosslinking density within each particle which, in turn, leads to a uniform polymer density in the swollen state. These more uniform particles, created by a semi-batch process, are more transparent in water than conventional (one-pot) microgel particles of the same size and concentration [25]. The reason for this difference in transparency is that the dense core (i.e., with higher crosslinker and polymer density) of the conventional (one-pot) particles tends to have a larger refractive index

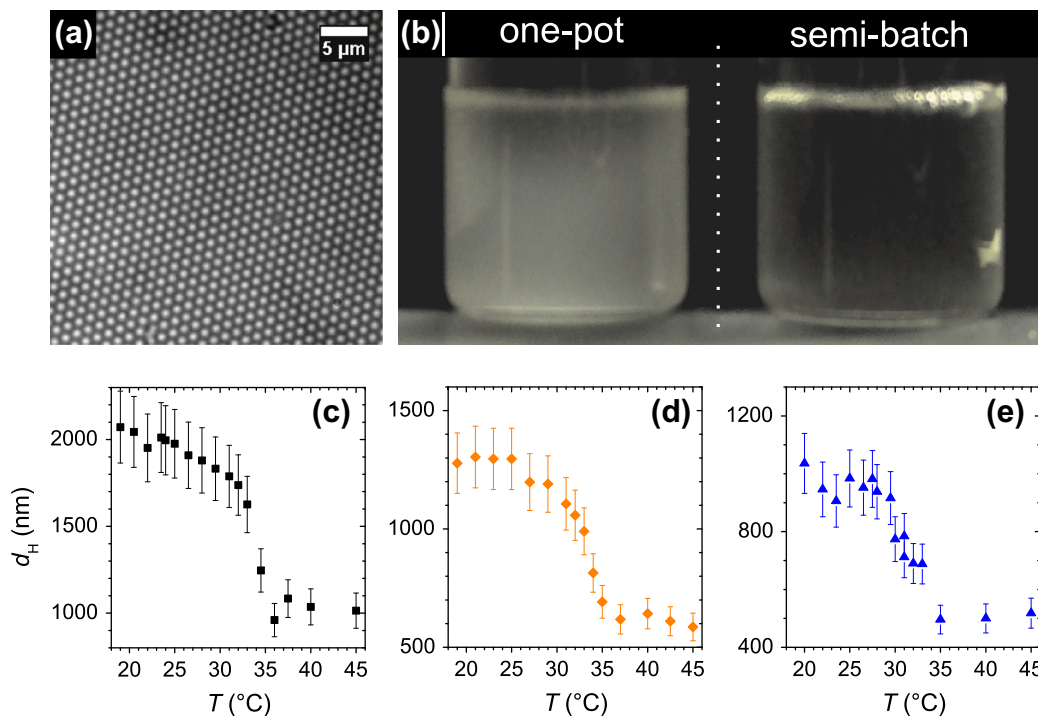


**Fig. 3.** (a) Quasi-two-dimensional colloidal crystal formed by PNIPAM spheres synthesized without AEMA and with NaCl. (b) Comparison between aqueous suspensions of PNIPAM spheres ( $d \approx 1.5 \mu\text{m}$ ) with volume fraction  $\phi_{\text{vol}} \approx 0.5\%$ , synthesized either by the classical one-pot synthesis (left) or by the feeding method (right). (c–e) Hydrodynamic diameter,  $d(T)$ , as a function of temperature as measured by dynamic light scattering for particles with AEMA (c), without AEMA and with NaCl (d), and with neither AEMA nor NaCl (e).

mismatch compared to the background solvent, i.e., a larger index and index-mismatch than the homogeneous particle. This larger refractive index mismatch leads to stronger light scattering and more suspension turbidity. The turbidity/transparency effect is apparent in Fig. 3b wherein we visualize two suspensions of PNIPAM particles with identical size and concentration ( $d \approx 1500 \text{ nm}$ ,  $\phi_{\text{vol}} \approx 0.5\%$ ), but synthesized by the conventional scheme versus the feeding method which produces homogeneous particles, respectively. A significant difference in transparency between the two samples is clearly evident.

Our transparency studies (Fig. 3b) provide evidence of the relatively weaker scattering of the homogeneous particles. Additional evidence for homogeneity can be derived from static light scattering measurements. Previous static light scattering experiments on smaller PNIPAM particles suggest that the density profile in the swollen state changes dramatically between one-pot and semi-batch syntheses. The “traditional” PNIPAM particles exhibit scattering signals that can be explained by a dramatic decrease in polymer density as one progresses from the center of the sphere towards its outer regions [39,38]. On the other hand, particles prepared by a semi-batch method are better described by an almost homogeneous polymer density distribution inside the spheres [24].

We have carried out light scattering experiments with our particles and have compared these data to models first developed to describe small angle neutron scattering by swollen microgel particles [37,24]. In brief, the model posits that the measured form factor,  $P(q)$  (with scattering wave vector  $q = 4\pi n_s/\lambda$ , where  $n_s$  is the refractive index of the solvent and  $\lambda$  the vacuum wavelength of the laser), is a product of the Rayleigh–Gans–Debye (RGD) approximation form factor with a Gaussian related to the variation in polymer density in the particle, i.e.,

$$P_{\text{hetero}}(q) = \left( \frac{3[\sin(qr) - qr \cos(qr)]}{(qr)^3} \exp\left(-\frac{(q\sigma_s)^2}{2}\right) \right)^2 \quad (1)$$

where  $r$  is the particle “core” radius, and  $\sigma_s$  is a characteristic length related to the decay in density. In real space, this corresponds to a radial profile that is homogeneous from the sphere’s center to a radial distance of  $r - 2\sigma_s$  and then decays smoothly up to the edge of the particle at radial distance  $r_{\text{sls}} = r + 2\sigma_s$  [37]. The polydispersity of the sample is also taken into account by averaging this form factor over an assumed Gaussian particle size distribution,  $D(r, \langle r \rangle, p)$ , i.e.,

$$P_{\text{hetero,poly}}(q) = \int_r D(r, \langle r \rangle, p) \times P_{\text{hetero}}(q, r) dr \quad (2)$$

with mean radius  $\langle r \rangle$  and polydispersity  $p$ .

We applied this model to characterize the scattering of our homogeneous PNIPAM hydrogel particles; the data for one ensemble of these spheres is shown in Fig. 4. The simple model provides a good fit of the data, and these results, in turn, are consistent with our other observations about the homogeneous particles, e.g., sample transparency and particle Brownian motion. The fitted “core-radius”  $r \approx 657 \pm 7 \text{ nm}$  is much larger than  $\sigma_s \approx 81 \pm 4 \text{ nm}$ <sup>1</sup>, which indicates that our particles are indeed relatively homogeneous; furthermore, the combined radius is  $r_{\text{sls}} = r + 2\sigma_s \approx 819 \pm 15 \text{ nm}$ , in good agreement with the hydrodynamic radius measured by dynamic light scattering,  $r_h = 828 \pm 21 \text{ nm}$ . We also verified the applicability of the approximation employed above by comparison with exact Mie calculations for the homogeneous sphere. Note, this check is carried out because our particles have radii on the order of magnitude of the laser wavelength, and therefore one of the conditions for the Rayleigh–Gans–Debye approximation is only marginally satisfied, i.e.,  $kd|1 - n_p/n_s| \ll 1$  (with  $k = 2\pi n_s/\lambda$  and  $n_p$  being the refractive index of the particles) [43]. The details of this comparison and

<sup>1</sup> Errors for the three fit parameters are calculated as the values that correspond to a relative change in goodness of fit not larger than 10% compared to the best fit, i.e.,  $\Delta\chi^2/\chi_{\text{min}}^2 \leq 0.1$ .

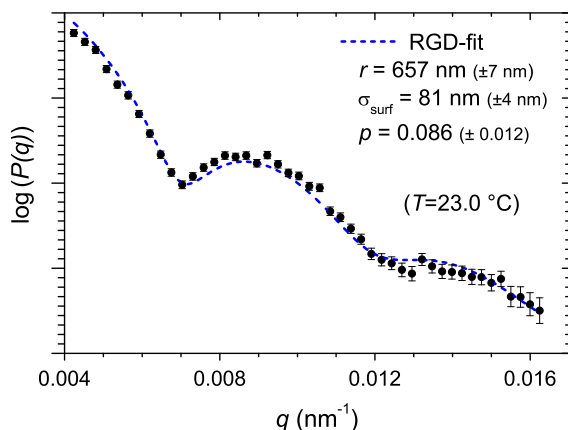


**Fig. 4.** Static light scattering data from a dilute aqueous suspension of semi-batch PNIPAM (with AEMA) and modified Rayleigh-Gans-Debye fit for inhomogeneous spheres as described in Eqs. (1) and (2).

approach, as well as comparison to a “traditional” PNIPAM particle of similar diameter, are provided in the supporting information.

### 3.3. Swelling behavior

The swelling behavior of different hydrogel particles is readily investigated by dynamic light scattering (DLS). Fig. 3c–e shows three  $d(T)$  curves for the three particle types shown in Fig. 2, i.e., with  $d(20\text{ °C}) \approx 1.0 - 2.1\ \mu\text{m}$ . All particles exhibit a slow decrease in  $d$  at low temperatures and a more rapid change between  $\approx 30$  and  $35\text{ °C}$ . At the highest temperatures studied, the particles are collapsed, and their diameters remain essentially constant.

It is commonly seen in colloidal microgels that the decrease in size around the lower critical mixing temperature  $\approx 32\text{ °C}$  is not perfectly sharp [13,20,25,44], i.e., not as sharp as is often observed for macroscopic PNIPAM gels. It is reasonable that the cross-linked charged colloids differ in their temperature-dependent phase behavior compared to that of the unconstrained PNIPAM-chains, and, clearly, crosslinking plays a role [13,44,45] in affecting the broadening of the transition. In order to develop a more detailed picture of the swelling behavior, further experiments probing the structural properties of the particles as a function of temperature are required. Future studies using temperature-dependent static light scattering experiments [32,24] could prove useful.

By comparing the particle diameter in the swollen state ( $20\text{ °C}$ ) to the diameter in the collapsed state ( $45\text{ °C}$ ), we determine the swelling ratios, which are given as  $d_{20\text{ °C}}/d_{45\text{ °C}}$  in Table 1. An important finding is that for the particles shown in Fig. 3c–e,  $d_{20\text{ °C}}/d_{45\text{ °C}} \approx 2.1$ . The ratio is essentially constant, i.e., the sign of the surface charge (positive with AEMA and negative without AEMA) does not significantly influence the swelling behavior. A slightly larger swelling ratio,  $d_{20\text{ °C}}/d_{45\text{ °C}} \approx 2.7$ , was measured for the largest particles (synthesis (b)). This increase could imply a lower polymer/water ratio in the swollen state compared to the polymer/water ratio in the smaller particles, or a corresponding lower relative water content in the collapsed state. As we pointed out earlier, relative water content is not readily determined; thus, we leave this point open for clarification by future experiments.

### 3.4. Summary

We have presented a colloidal synthesis method for large colloidal PNIPAM hydrogel particles via a surfactant-free semi-batch emulsion polymerization. Our approach builds upon previous methods and is useful because particle diameter can be easily adjusted over a wide range between  $d \approx 0.8 - 4\ \mu\text{m}$ , and because

continuous feeding of monomer and crosslinker produces thermo-sensitive particles with uniform crosslinking density and uniform refractive index. The crucial parameter for controlling the particle size is the charge concentration on the seed surface shortly after initiation. Thus, variation of electrolyte concentration, addition of small amounts of positively charged co-monomer, as well as control of the amount of fed monomer, all help facilitate systematic control of particle size.

### Acknowledgments

We thank Peter Collings for assistance with the static light scattering measurements, Paul Janmey and Katrina Cruz for access to the dynamic light scattering setup, and Kwadwo Tettey for help with the zeta potential measurements. We gratefully acknowledge financial support from the National Science Foundation through DMR12-05463 and DMR-1206231 (K.B.A.), the PENN MRSEC DMR11-20901, and NASA NNX08AO0G. T.S. acknowledges financial support from DAAD.

### Appendix A. Supplementary material

Supplementary data associated with this article can be found, in the online version, at <http://dx.doi.org/10.1016/j.jcis.2013.05.042>.

### References

- [1] D. Schmaljohann, *Adv. Drug Deliv. Rev.* 58 (15) (2006) 1655–1670.
- [2] I. Varga, I. Szalai, R. Mszaros, T. Gilnyi, *J. Phys. Chem. B* 110 (41) (2006) 20297–20301.
- [3] G.E. Morris, B. Vincent, M.J. Snowden, *Prog. Colloid Polym. Sci.* 105 (1997) 16.
- [4] Q. Luo, Y. Guan, Y. Zhang, M. Siddiq, *J. Polym. Sci. Part A Polym. Chem.* 48 (18) (2010) 4120–4127.
- [5] A.M. Alsayed, M.F. Islam, J. Zhang, P.J. Collings, A.G. Yodh, *Science* 309 (5738) (2005) 1207–1210.
- [6] Y. Han, Y. Shokef, A.M. Alsayed, P. Yunker, T.C. Lubensky, A.G. Yodh, *Nature* 456 (2008) 898–903.
- [7] J. Mattsson, H.M. Wyss, A. Fernandez-Nieves, K. Miyazaki, Z. Hu, D.R. Reichman, D.A. Weitz, *Nature* 462 (7269) (2009) 83–86.
- [8] K.-Q. Zhang, X.Y. Liu, *Langmuir* 25 (2009) 5432.
- [9] P. Yunker, Z. Zhang, A.G. Yodh, *Phys. Rev. Lett.* 104 (2010) 015701.
- [10] Z. Wang, W. Qi, Y. Peng, A.M. Alsayed, Y. Chen, P. Tong, Y. Han, *J. Chem. Phys.* 134 (3) (2011) 034506.
- [11] Y. Peng, Z. Wang, Y. Han, *J. Phys. Conf. Ser.* 319 (1) (2011) 012010.
- [12] D.O. Kiminta, P. Luckham, S. Lenon, *Polymer* 36 (25) (1995) 4827–4831.
- [13] R. Pelton, *Adv. Colloid Interf. Sci.* 85 (1) (2000) 1–33.
- [14] B.R. Saunders, *Langmuir* 20 (10) (2004) 3925–3932.
- [15] B.R. Saunders, N. Laajam, E. Daly, S. Teow, X. Hu, R. Stepto, *Adv. Colloid Interf. Sci.* 147–148 (0) (2009) 251–262.
- [16] H. Senff, W. Richtering, *J. Chem. Phys.* 111 (1999) 1705.
- [17] H. Senff, W. Richtering, *Colloid. Polym. Sci.* 278 (2000) 830–840.
- [18] E.H. Purnomo, D. van den Ende, S.A. Vanapalli, F. Mugele, *Phys. Rev. Lett.* 101 (2008) 238301.
- [19] K.N. Nordstrom, E. Verneuil, P.E. Arratia, A. Basu, Z. Zhang, A.G. Yodh, J.P. Gollub, D.J. Durian, *Phys. Rev. Lett.* 105 (17) (2010) 175701.
- [20] G.R. Deen, T. Alsted, W. Richtering, J.S. Pedersen, *Phys. Chem. Chem. Phys.* 13 (2011) 3108–3114.
- [21] C. Scherzinger, O. Holderer, D. Richter, W. Richtering, *Phys. Chem. Chem. Phys.* 14 (2012) 2762–2768.
- [22] F.A. Plamper, A.A. Steinschulte, C.H. Hofmann, N. Drude, O. Mergel, C. Herbert, M. Erberich, B. Schulte, R. Winter, W. Richtering, *Macromolecules* 45 (19) (2012) 8021–8026.
- [23] X. Wu, R.H. Pelton, A.E. Hamielec, D.R. Woods, W. McPhee, *Colloid Polym. Sci.* 272 (1994) 467–477.
- [24] S. Meyer, W. Richtering, *Macromolecules* 38 (4) (2005) 1517–1519.
- [25] R. Acciaro, T. Gilányi, I. Varga, *Langmuir* 27 (12) (2011) 7917–7925.
- [26] H. Shimizu, R. Wada, M. Okabe, *Polym. J.* 41 (9) (2009) 771–777.
- [27] Z. Meng, J.K. Cho, V. Breedveld, L.A. Lyon, *J. Phys. Chem. B* 113 (2009) 4590–4599.
- [28] A.N. St. John, V. Breedveld, L.A. Lyon, *J. Phys. Chem. B* 111 (2007) 7796–7801.
- [29] A.M. Alsayed, Y. Han, A. Yodh, *Microgel Suspensions*, Wiley-VCH, Weinheim, 2011. Ch. Melting and geometric frustration in temperature-sensitive colloids, pp. 229–281.
- [30] F. Meunier, A. Elaissari, C. Pichot, *Polym. Adv. Technol.* 6 (7) (1995) 489–496.
- [31] A.F. Routh, B. Vincent, *Langmuir* 18 (14) (2002) 5366–5369.
- [32] C. Wu, S. Zhou, S.C.F. Au-yeung, S. Jiang, *Angew. Makromol. Chem.* 240 (1996) 123.

- [33] A.K. Lele, M.M. Hirve, M.V. Badiger, R.A. Mashelkar, *Macromolecules* 30 (1997) 157.
- [34] J.C. Crocker, D.G. Grier, *J. Colloid. Int. Sci.* 179 (1996) 298.
- [35] K. Kratz, T. Hellweg, W. Eimer, *Polymer* 42 (15) (2001) 6631–6639.
- [36] A. Fernández-Barbero, A. Fernández-Nieves, I. Grillo, E. López-Cabarcos, *Phys. Rev. E* 66 (2002) 051803.
- [37] M. Stieger, W. Richtering, J.S. Pedersen, P. Lindner, *J. Chem. Phys.* 120 (13) (2004) 6197–6206.
- [38] T.G. Mason, M.Y. Lin, *Phys. Rev. E* 71 (2005) 040801.
- [39] M. Reufer, P. Diaz-Leyva, F. Scheffold, *Eur. Phys. J. E* 28 (2009) 165.
- [40] R.H. Pelton, H.M. Pelton, A. Morphesis, R.L. Rowell, *Langmuir* 5 (3) (1989) 816–818.
- [41] B.R. Saunders, B. Vincent, *Adv. Colloid Interf. Sci.* 80 (1999) 1–25.
- [42] T. Hoare, D. McLean, *J. Phys. Chem. B* 110 (41) (2006) 20327–20336.
- [43] C.F. Bohren, D.R. Huffman, *Absorption and Scattering of Light by Small Particles*, Wiley Science Paperback Series, John Wiley & Sons, Inc., 1998.
- [44] Y. Deng, W. Yang, C. Wang, S. Fu, *Adv. Mater.* 15 (20) (2003) 1729–1732.
- [45] W. McPhee, K.C. Tam, R. Pelton, *J. Colloid Int. Sci.* 156 (1993) 24.